NON-DESTRUCTIVE TEXTURAL AND MINERALOGICAL CHARACTERISATION OF NANOMETRIC INCLUSIONS WITHIN METEORITE SAMPLES BY COMBINING X-RAY COMPUTED TOMOGRAPHY AND REFLECTANCE SPECTROSCOPY. P-E. M. C. Martin[1], R. Ottersberg[1], A. Pommerol[1], I. Leya[1], H. Busemann[2], O-Z. Khoma[3], D. Haberthür[3], and R. Hlushchuk[3]. [1]Space Research and Planetary Sciences, Physics Institute, University of Bern, Bern, Switzerland. [2]Institute of Geochemistry and Petrology, ETH Zürich, Switzerland. [3]Institute of Anatomy, University of Bern, Bern, Switzerland. (pierre-etienne.martin@unibe.ch).

Introduction: Identifying and characterising nanometre-scale inclusions found within asteroidal and Martian samples key insights into early Solar System processes and the delivery of prebiotic material to Earth [1–5]. Nano-X-ray Computed Tomography (nano-XCT) enables the non-destructive [6] 3D visualisation of the internal structure of samples (cf. Fig. 1A) and extraction of specific regions of interest (cf. Fig. 1B). However, nano-XCT datasets are primarily based on X-ray absorption contrast, which can limit phase discrimination when materials of similar density are present (e.g. glassy Martian inclusions versus feldspar). To address this limitation, visible and Near-Infrared (NIR) reflectance spectroscopy were integrated to provide complementary surface mineralogical information for targeted regions of interest (cf. Fig. 1C). Through correlation and interpolation between volumetric nano-XCT data and spectroscopic measurements, this combined approach enables robust phase identification within meteoritic samples despite their small size (mm- and sub-mm-long) and relatively low reflectance. The integration of nano-XCT and NIR spectroscopy therefore could provide a novel approach to non-destructive mineral identification and improved sample interpretation. Only results from analyses of the NWA 16272 Martian meteorite are presented here. However, the complete study includes additional Martian meteorites (Chassigny, Nakhla, and Tissint), as well as carbonaceous chondrites used as asteroid analogues (Cold Bokkeveld, Mighei, and Orgueil).

Material and Methods: Nano-XCT imaging was conducted using a Bruker SKYSCAN 2214 at the Institute of Anatomy at the University of Bern. The instrument can achieve a true 3D resolution of 500 nm and a voxel size of 60 nm. Data processing and visualisation were performed using the CT Vox and the Dragonfly 3D software. Visible reflectance spectra (400–1040 nm) and NIR spectra (850–2500 nm) were acquired using an updated version of the Mobile Hyperspectral Imaging System [MoHIS; 7] at the University of Bern.

Results: NWA 16272 is a highly vesicular Martian basalt [8]. The analysed sample (AF-3), on loan from ETH Zurich, weighs 61.8 mg and measures approximately 5.9 × 3.6 mm.

Nano-XCT imaging. The sample surface features a spinifex texture (cf. Fig. 1A). 3D segmentation (cf. Fig. 1B) reveals that the porosity accounts for ~0.01% (~0.02 mm^3) of the total sample volume. Vesicles range from <5 µm to ~100 µm in length. No global preferential orientation is observed, although a few elongated vesicles are present. The glassy inclusion (contoured in red; cf. Fig. 1) is relatively non-porous.

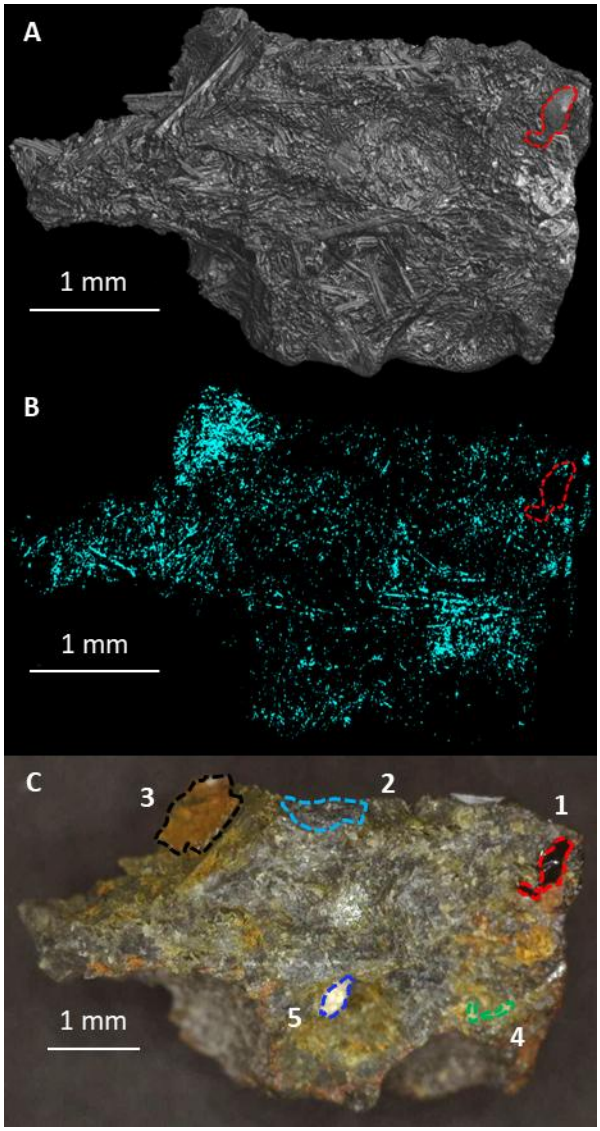

Fig. 1. *(**A**) Greyscale render of the nano-XCT 3D scan of the NWA 16272,AF-3 sample, acquired at 60 kV with a voxel size of 2 µm. Brighter phases correspond to minerals with higher X-ray absorption capacity which indicates a higher density. An identified glassy inclusion is outlined in red dashed lines. (**B**) Internal porosity segmented using the model developed by [9]. (**C**) Optical photograph of the*

sample at a 50× magnification, highlighting the targeted mineral phases of interest for spectroscopic analysis.

Reflectance spectroscopy. The spectrum of ROI 1 (red; cf. Fig. 2) corresponds to glass, characterised by its very low reflectance and the absence of absorption features, consistent with the amorphous (opaque) nature of the phase. ROI 2, (turquoise; cf. Fig. 2), despite being relatively featureless, presents higher reflectance levels which would be expected from plagioclase. ROI 3 (black; cf. Fig. 2) likely represents a mixture of pyroxene and lower-reflectance assemblages (e.g. basaltic mesostasis), displaying narrow absorption features at ~1.0 and ~2.0 µm. ROI 4 (green; cf. Fig. 2) shows broad absorption features near 0.9, 1.0, and 1.3 µm, which correspond to olivine. ROI 5 (blue; cf. Fig. 2) is characterised by broad absorption features, each centred around 0.95 µm and 1.95 µm, characteristic of pyroxene. Spectral interpretations were supported through comparison with the RELAB spectral library. Discrepancies between the visible and NIR spectra are primarily due to viewing geometry.

Discussion: This correlative workflow combines volumetric textural and surface mineralogical datasets, enabling the characterisation of both surface and subsurface regions of interest. Glassy inclusions identified in Martian meteorites could be targeted for noble gas analyses (particularly Ne) to provide key constraints regarding the composition of the paleo-environment and atmospheric evolution of Mars [11–14]. Further data processing is required to isolate glass inclusions and other phases of interest from the nano-XCT datasets. Additionally, measured reflectance spectra could also be compared with remote-sensing datasets from Mars and C-type asteroids, facilitating reconstruction of sample histories [e.g. 15]. Spectral data acquisition will also be further improved with better calibration (e.g. non-linearity correction of the lock-in algorithm) to strengthen this approach. This project aims to establish a non-destructive correlative methodology capable of spatially resolving, detecting, and characterising sub-micrometre phases in Martian meteorites, carbonaceous chondrites, and asteroid-returned samples. The resulting protocols could also directly support future Martian and asteroidal sample-return missions.

References: [1] Parker E. T. et al. (2023) *GCA* 347:42–57. [2] Potiszil C. et al. (2023) *Nat. Commun.* 14:1482. [3] Glavin D. P. et al. (2025) *Nat. Astron.* 9:199–210. [4] De Gregorio B. T. (2015) In *Encyclopedia of Astrobiology* 990–991. [5] Mathurin J. et al. (2024) *A&A* 684:A198. [6] Ghaznavi P. et al. (2023) *M&PS* 58 (6):897–900. [7] Cerubini, R. et al. (2022) *P&SS* 211, 105391. [8] Gattacceca, J. et al. (2024) *M&PS* 59: 1820-1823. [9] Taute, C. et al. (2021) *J. South. Afr. Inst. Min. Metall.* 121(4):143-150. [10] Wiens R. C. et al. (1986) *EPSL* 77 (2):149–158. [11] Wiens R. C. (1988) *EPSL* 91 (1-2):55–65. [12] Wieler R. et al. (2016) *M&PS* 51 (2):407–428. [13] Bogard D. D. et al. (1998) *GCA* 62 (10):1829–1835. [14] Crowther S. A. et al. (2022) *GCA* 336:372–393. [15] Simon et al. (2020) *A&A* 644:A148.

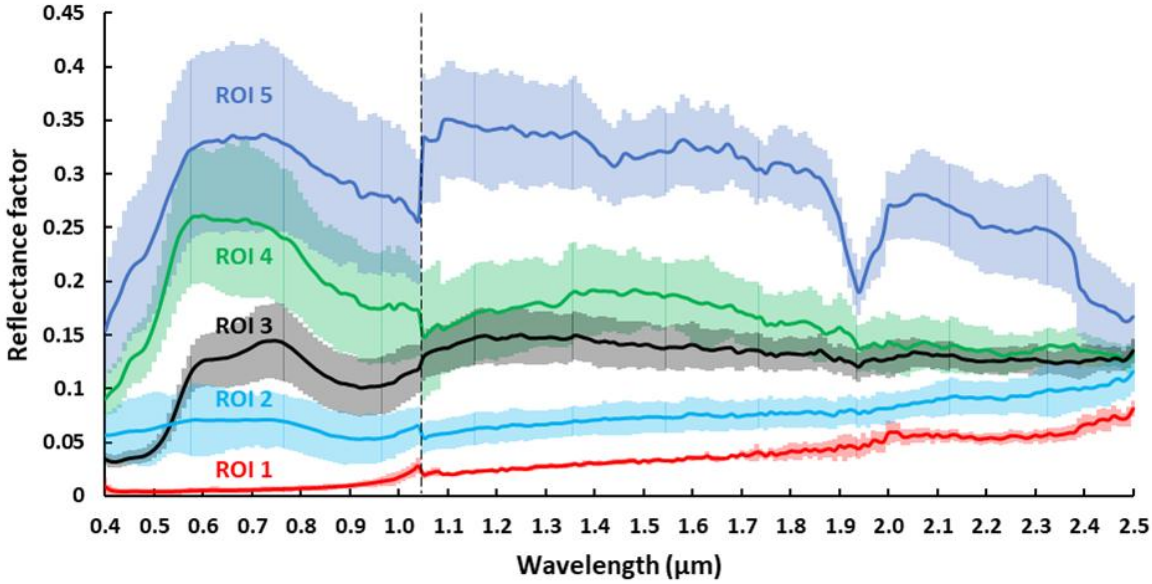

Fig. 2. *Mean visible and NIR reflectance spectra (Reflectance Factor, REFF) of the selected regions of interest (ROIs) within the mineral phases of the NWA 16272 sample, displayed in Fig. 1C. Standard deviation for each spectrum is represented as a shaded area. The dotted line corresponds to a change in filters/detectors, and the resulting steps near 1.4 µm should be considered artefacts. Spectra were acquired with a 10 nm sampling and a spectral resolution of 10.8-21.6 nm and were smoothed to improve clarity.*